

# Investigation of the Radial Profile of Galactic Magnetic Fields using Rotation Measure of Background Quasars

Paras Sharma,<sup>1</sup>  Shivam Burman,<sup>1</sup>  Sunil Malik,<sup>2,3</sup>  and Suprit Singh<sup>1</sup> 

<sup>1</sup>Indian Institute of Technology Delhi, Hauz Khas, New Delhi, Delhi 110016, India

<sup>2</sup>Institute für Physik und Astronomie Universität Potsdam, Golm Haus 28, D-14476 Potsdam, Germany

<sup>3</sup>Deutsches Elektronen-Synchrotron DESY, Platanenallee 6, 15738 Zeuthen, Germany

Accepted XXX. Received YYY; in original form ZZZ

## ABSTRACT

Probing magnetic fields in high-redshift galactic systems is crucial to investigate galactic dynamics and evolution. Utilizing the rotation measure of the background quasars, we have developed a radial profile of the magnetic field in a typical high- $z$  galaxy. We have compiled a catalog of 59 confirmed quasar sightlines, having one intervening Mg II absorber in the redshift range  $0.372 \leq z_{\text{abs}} \leq 0.8$ . The presence of the foreground galaxy is ensured by comparing the photometric and spectroscopic redshifts within  $3\sigma_{z-\text{photo}}$  and visual checks. These quasar line-of-sights (LoS) pass through various impact parameters ( $D$ ) up to 160 kpc, covering the circumgalactic medium of a typical Milky-Way type galaxy. Utilizing the residual rotation measure (RRM) of these sightlines, we estimated the excess in RRM dispersion,  $\sigma_{\text{ex}}^{\text{RRM}}$ . We found that the sightlines having impact parameters  $D \leq 50$  kpc and  $D > 50$  kpc,  $\sigma_{\text{ex}}^{\text{RRM}}$  show significant difference from  $24.86 \pm 3.08$  rad m<sup>-2</sup> to  $16.34 \pm 1.88$  rad m<sup>-2</sup> respectively. The profile of  $\sigma_{\text{ex}}^{\text{RRM}}$  with  $D$  exhibits a decreasing trend. We translated  $\sigma_{\text{ex}}^{\text{RRM}}$  to average LoS magnetic field strength,  $\langle B_{\parallel} \rangle$  by considering a typical electron column density. Consequently, the anti-correlation is sustained, resulting in a decreasing magnetic field profile. This suggests a clear indication of varying magnetic field from the disk to the circumgalactic medium. This work provides a methodology that, when applied to ongoing and future radio polarisation surveys such as LOFAR and SKA, promises to significantly enhance our understanding of magnetic field mapping in galactic systems.

**Key words:** galaxies: haloes, high-redshift, magnetic fields, quasars: general, absorption lines

## 1 INTRODUCTION

Galactic magnetic fields play a pivotal role in a variety of astrophysical phenomena, such as governing star formation, influencing the dynamics and stability of the interstellar medium, and even in instigating galactic winds (see refs. Ruzmaikin et al. 1988; Shu 1992; Beck 2005; Brandenburg & Subramanian 2005; Krumholz et al. 2011; Crutcher 2012; Beck & Wielebinski 2013; Klein & Fletcher 2015). An important role in the galactic evolution and dynamics is also played by the inflow and outflow of material from a galaxy to its circumgalactic medium (CGM) (see the review by Tumlinson et al. 2017). The CGM remains one of the least constrained parts of the galactic systems, especially with regard to the magnetic fields. At high redshifts, the galactic magnetic fields gain a cosmological perspective with questions such as the generation (see refs. Rees 1987; Kulsrud et al. 1997; Seta & Federrath 2020) and sustenance mechanisms of magnetic fields in the galactic systems over several epochs

during their evolution (Widrow 2002; Subramanian 2008; Rieder & Teyssier 2016). It is, therefore, vital to probe the strength, structure, and evolution of magnetic fields in galaxies and their CGM to gain insights into galactic dynamics and evolution.

There are numerous investigations on the structure and strength of magnetic fields in the Milky Way and the nearby galaxies such as M31 (see refs. Jansson & Farrar 2012; Han 2012; Gießübel, R. et al. 2013; Beck 2015; Beck, Rainer 2015; Khoperskov, Sergey A. & Khrapov, Sergey S. 2018; Seta & Federrath 2021; Dickey et al. 2022; Surgent et al. 2023). The average magnetic field strength over the galactic scales ranges from 0.5 to 2.5  $\mu\text{G}$  and follows a decreasing trend towards the galaxy outskirts (up to  $\sim 25$  kpc). Studies on the CGM of galaxies have shown that the CGM hosts magnetic fields up to significantly large distances up to 1000 kpc from the galactic centers. (see refs. Henriksen & Irwin 2016; Mora-Partiarroyo et al. 2019; van de Voort et al. 2021; Thomas et al. 2022; Heesen, V. et al. 2023; Böckmann, K. et al. 2023). In addition, Heesen, V. et al. (2023) have studied the CGM magnetic fields in the nearby galaxies (lying within 3.2-109 Mpc distance from the Milky Way), having an impact parameter (transverse distance from galaxy center to the line of sight) distribution up to 1000 kpc, using LOFAR observations at 144 MHz.

\* sharmaparasiitd@gmail.com

† shivam5268@gmail.com

‡ sunil.malik@uni-potsdam.de

§ suprit@iitd.ac.in

The authors estimated the average strength of the line-of-sight (LoS) component of the magnetic field of  $0.5\mu\text{G}$ .

For the galaxies at high redshifts, particularly the Rotation Measures (RM) of polarized radio quasars have been employed extensively to investigate the magnetic fields whenever these systems occur along the quasar sightlines (Kronberg & Perry 1982; Kronberg et al. 2008). Being an integrated LoS effect, the observed quasar  $\text{RM}_{\text{obs}}$  includes the intrinsic contribution of (i) the source and its host itself ( $\text{RM}_{\text{qso}}$ ), (ii) the intergalactic medium (IGM) ( $\text{RM}_{\text{IGM}}$ ), (iii) the intervening galactic systems ( $\text{RM}_{\text{intrv}}$ ), and (iv) the Milky Way (GRM) all added up. Note, however, that RM can be negative or positive, as it depends on the mean strength of the magnetic field in the elements along the LoS. The occurrence of intervening systems in the LoS is detected through the absorption lines in the quasar spectra. In particular, the Mg II absorption doublets 2796, 2803 Å have shown a high degree of correlation with the normal galaxies occurring at the same redshifts as these absorbers (see refs. Churchill et al. 2000; Nestor et al. 2005; Mshar et al. 2007; Narayanan et al. 2008; Tinker & Chen 2010). These Mg II absorbers can be traced up to the extent greater than 100 Kpc from the center of galaxy (see refs. Kacprzak et al. 2008; Chen et al. 2010; Bordoloi et al. 2011; Nielsen et al. 2013). An excess RM has been observed for all the quasar sightlines with Mg II absorbers in the spectra compared to those showing no absorbers. In order to obtain the RM contribution from the intervening systems, all other contributions need to be removed carefully, as there are also directional dependencies, particularly in the GRM. The estimates of the magnetic fields in the intervening systems are thus obtained from the Residual Rotation Measure ( $\text{RRM} = \text{RM} - \text{GRM}$ ) statistics where the GRM contribution has been removed (see refs. Bergeron & Boissé 1991; Kronberg et al. 2008; Bernet et al. 2010, 2012; Hammond et al. 2013; Joshi & Chand 2013; Farnes et al. 2014; Kim et al. 2016). Using these techniques, for example, Malik et al. (2020) gave an estimated average LoS magnetic field to be around  $1.3 \pm 0.3\mu\text{G}$ . Recently an article by Böckmann, K. et al. (2023) appeared where the authors have examined the magnetic fields properties in the CGM of 125 star-forming galaxies in the COSMOS<sup>1</sup> (81 galaxies having spectroscopic redshift in the range 0.25-0.49) and XMM-LSS<sup>2</sup> (44 galaxies having spectroscopic redshift in the range 0.06-1.09) fields, using the polarization data from the MeerKAT International GHz Tiered Extragalactic Exploration polarization (MIGHTEE-POL) survey, extensively provided by Taylor et al. (2023). The authors obtained a redshift corrected excess  $|\text{RM}|$  of  $5.6 \pm 2.3 \text{ rad m}^{-2}$  for the galaxies having impact parameter less than 133 kpc from the background radio source, with respect to the galaxies having impact parameter between the range 133-400 kpc.

While models and simulations of the structural aspects of magnetic fields in galaxies and their halos exist (see refs. Pakmor et al. 2020; Thomas et al. 2022; Jung et al. 2023) in the literature, these structures remain largely unexplored from an observational standpoint. In one study Bernet et al. (2013) analyzed 28 sources with RM values at 6 cm and concluded that the sightlines with higher values of RM have small impact parameters, following a decreasing profile up to  $\sim 50$  kpc with  $O(B_{\parallel}) \sim 10 \mu\text{G}$ . Also, Lan & Prochaska (2020) have reported the analysis of around 1000 high- $z$  galaxies with impact parameters up to 200 kpc and found that the RM is uncorrelated with the number of intervening galaxies along the LoS, and constrained the CGM magnetic field to be less than  $2\mu\text{G}$ . The question lies open

**Table 1.** Table of Physical quantities used in this article.

| Symbol                                   | Description  |
|--|--|
| RM                                       | Rotation measure   |
| GRM                                      | Galactic Rotation measure  |
| IGM                                      | Intergalactic medium   |
| $\text{RM}_{\text{qso}}$                 | Rotation measure of host quasar  |
| CGM                                      | Circumgalactic Medium  |
| RRM                                      | Residual Rotation measure  |
| $B_{\parallel}$                          | Magnetic field component parallel to the line of sight                     |
| $z_{\text{qso}}$                         | Redshift of the background quasar  |
| $z_{\text{abs}}$                         | Spectroscopic redshift of the MgII absorber                                |
| $z_{\text{gal(photo)}}$                  | Photometric redshift of intervening galaxy                                 |
| $b$                                      | Galactic latitude  |
| $\sigma_{z-\text{photo}}$                | Uncertainty in photometric redshift  |
| $\theta$                                 | Angular separation   |
| $\Delta\delta$                           | Declination separation among the background quasar and absorber galaxy     |
| $\Delta\alpha$                           | Right ascension separation among the background quasar and absorber galaxy |
| $\delta_{\text{qso}}$                    | Declination of the background quasar                                       |
| $D$                                      | Impact parameter (in kpc)  |
| $d_A$                                    | Angular diameter distance  |
| $H_0$                                    | Hubble constant  |
| $\Omega_m$                               | Matter density   |
| $\Omega_\Lambda$                         | Cosmological constant  |
| $\sigma_{\text{RRM}}^{\text{abs}}$       | RRM dispersion of absorbers in each D bin                                  |
| $\text{RRM}_{\text{non-abs}}$            | RRM of the non-absorber sightlines   |
| $\sigma_{\text{RRM}}^{\text{non-abs}}$   | RRM dispersion of non-absorber sightlines                                  |
| $N_b$                                    | Number of quasar-galaxy pairs in each D bin                                |
| $\delta\sigma_{\text{RRM}}^{\text{abs}}$ | Uncertainty in the RRM dispersion of the absorbers                         |
| $\rho\rho$                               | Pearson correlation coefficient  |
| $\sigma_{\text{RRM}}^{\text{ex}}$        | Excess RRM due to intervening absorbers for each D bin                     |
| $\delta\sigma_{\text{RRM}}^{\text{ex}}$  | Uncertainty in the $\sigma_{\text{RRM}}^{\text{ex}}$                       |
| $N_e$                                    | Column density of electrons  |
| $\sigma_{\text{RRM}}^{\text{abs(sim)}}$  | Excess RRM estimated using simulated data                                  |

as to what is the structure and profile of the magnetic fields in these high- $z$  galaxies?

We consider this question statistically by first identifying an ensemble of quasar-galaxy pairs through Mg II absorbers and a visual check in the Sloan Digital Sky Survey (SDSS) catalogs. Using the angular separation between the quasar LoS and the center of the intervening galaxies, we can compute the impact parameters of the sightlines. We obtain the excess contribution in RRM ( $\sigma_{\text{RRM}}^{\text{ex}}$ ) due to the intervening galaxy by comparing the dispersion of RRM distributions of the quasar sightlines with and without absorbers. The column average strength of the LoS component of the magnetic field can then be estimated from this excess RRM. We can then answer the question posed above by seeking the correlation of the obtained magnetic fields with the impact parameters of the sources by assuming all the intervening galaxies to be similar, marginalizing their properties as a preliminary stride in the direction of profiling the magnetic fields in these galactic systems.

This paper is organized as follows. We begin with characterizing the dataset and building our sample in Section 2. The details of our analysis, including the estimation of the impact parameter of the quasar-galaxy pairs, the radial profile of rotation measure, and the estimated magnetic field, are given in Section 3. A detailed discussion of our results, as well as a comparison with previous studies, is given in Section 4. We conclude the paper by summarizing our findings in Section 5.

## 2 DATA AND SAMPLE CREATION

In our study, we have employed the catalog of 1132 well-studied quasars compiled by Malik et al. (2020) derived from a positional cross-match of Sloan Digital Sky Survey Data Release (SDSS DR)-7, 9, 12, 14 quasar catalogs (Abazajian et al. 2009; Ahn et al. 2012; Alam et al. 2015; Abolfathi et al. 2018) with the NRAO VLA Sky Survey (NVSS) RM-21cm catalog (Taylor et al. 2009). In this compilation, intervening galaxies along the LoS are reported through the Mg II

<sup>1</sup> <https://cosmos.astro.caltech.edu/>

<sup>2</sup> <https://cesam.lam.fr/xmm-lss/>

**Table 2.** The table shows the required parameters of the quasar-galaxy pairs in our sample. The last column represents the impact parameter, ‘D’, between the LoS of the quasar from the center of the intervening galaxies, which is confirmed by photometric and spectroscopic observations. The complete table containing all 59 galaxy-quasar pairs is available in machine-readable form.

| QSO                  | GAL                  | RM                  | $\delta$ RM         | RRM                 | $\delta$ RRM        | $z_{\text{qso}}$ | $z_{\text{abs}}$ | $z_{\text{gal}}$ (photo) | $\sigma_{z-\text{photo}}$ | D     |
|----------------------|----------------------|---------------------|---------------------|---------------------|---------------------|------------------|------------------|--------------------------|---------------------------|-------|
| Jhhmss.xx±ddmmss.xx  | Jhhmss.xx±ddmmss.xx  | rad m <sup>-2</sup> | rad m <sup>-2</sup> | rad m <sup>-2</sup> | rad m <sup>-2</sup> | spec             | spec             | photo                    | photo                     | kpc   |
| J154459.43+040746.37 | J154459.45+040750.82 | 22.1                | 4.4                 | 14.4                | 4.6                 | 2.1881           | 0.42             | 0.339                    | 0.0959                    | 25.43 |
| J140918.82+645521.49 | J140918.26+645525.09 | 45.2                | 13.7                | 16.0                | 13.8                | 1.0312           | 0.431            | 0.362                    | 0.0486                    | 29.21 |
| J234831.77+062459.69 | J234831.99+062504.33 | 38.8                | 4.8                 | 40.3                | 5.0                 | 1.5396           | 0.38             | 0.413                    | 0.0863                    | 30.66 |
| J102444.80+191220.42 | J102445.07+191223.73 | 25.6                | 5.5                 | 18.4                | 5.7                 | 0.8275           | 0.528            | 0.554                    | 0.0349                    | 32.59 |
| J135726.48+001542.42 | J135726.17+001539.73 | -13.3               | 10.6                | -14.6               | 10.7                | 0.6614           | 0.477            | 0.42                     | 0.1112                    | 32.95 |
| J083052.09+241059.82 | J083052.51+241101.94 | 12.0                | 0.9                 | -5.2                | 1.7                 | 0.9414           | 0.525            | 0.419                    | 0.0495                    | 39.6  |
| ⋮                    | ⋮                    | ⋮                   | ⋮                   | ⋮                   | ⋮                   | ⋮                | ⋮                | ⋮                        | ⋮                         | ⋮     |

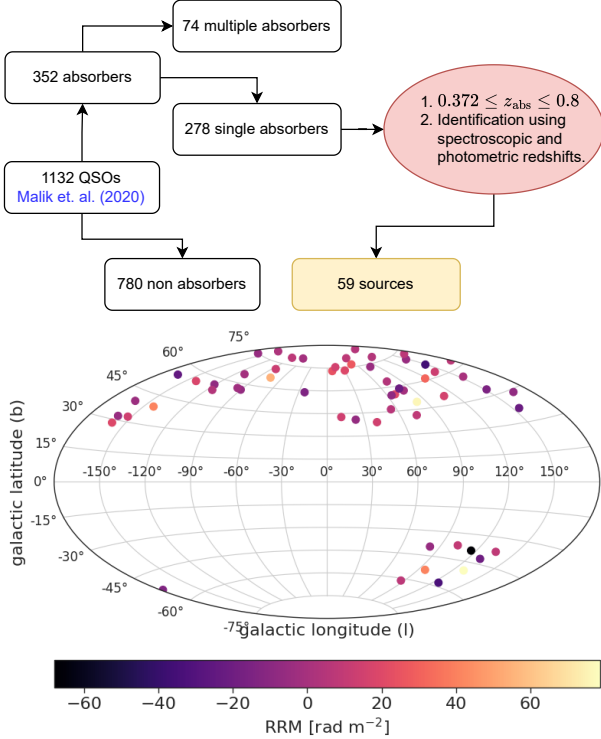


**Figure 1.** *Top Panel:* Illustration of the sample generation procedure for extracting the final sample for 59 sightlines. *Bottom Panel:* Location of the 59 galaxy-quasar pairs in the galactic coordinates, color-coded with the RRM values.

$\lambda 2796, 2803 \text{ \AA}$  doublet absorption lines in the quasar spectra. This criterion, combined with the wavelength coverage of SDSS, 3800–9000  $\text{\AA}$ , selects only the absorbers lying within the redshift range of  $0.372 \leq z_{\text{abs}} \leq 2.2$ . A positional cross-match of the catalogs has been performed with a vicinity radius of  $7''$  due to the different spatial resolutions of the optical and radio telescopes. This threshold radius is identified based on localization uncertainties of telescopes involved in these catalogs and has also been investigated in Kimball & Željko Ivezić (2008) and Singh & Chand (2018). The compilation contains all the necessary observed and derived quantities, including the RRM where the contribution of the RM from the Milky Way has been removed. To segregate the sightlines based on the presence and the absence of the intervening Mg II absorbers, the authors have also used visual identification by investigating the individual spectrum of the quasars. The catalog comprises of 352 sightlines with single and multiple intervening Mg II absorbers and 780 sightlines without

any intervening absorber (hereafter non-absorber sightlines). The background quasars corresponding to the absorber and non-absorber sightlines lie within the redshift range of  $0.421 \leq z_{\text{qso}} \leq 2.298$  and  $0.388 \leq z_{\text{qso}} \leq 2.298$ , respectively.

With the aim to infer the radial profile of the magnetic field in these intervening galaxies/absorbers, we take up the 352 sightlines having single/multiple absorbers in their foreground. As mentioned above, the absorbers can be in the redshift range of  $0.372 \leq z_{\text{abs}} \leq 2.2$ . We now lay down the detailed filtering procedure to extract our final sample of 59 sightlines having only one absorber (see top panel of Fig. 1). The procedure is as follows:

- (i) To reduce the degeneracy among the contribution in excess RM from multiple absorbers, we selected 278 sightlines having a single absorber out of the initial sub-sample of 352 sources containing absorbers in the foreground.
- (ii) To ensure both the quasar and absorber galaxy are resolvable in the photometric data, we restricted our analysis to intervening galaxies with redshift  $z_{\text{abs}} \leq 0.8$ , narrowing down our selection to 112 sources within this redshift range. The upper limit is also constrained by the telescope’s limited magnitude and spatial photometric resolution.
- (iii) We retrieved the photometric images of these 112 sources from the SDSS DR16 Skyserver<sup>3</sup> and searched for nearby galaxies with the photometric redshift consistent with the spectroscopic redshift to within a  $3\sigma_{z-\text{photo}}$  range. Here,  $\sigma_{z-\text{photo}}$  represents the uncertainty in the photometric redshift of the galaxy. Using this technique, we successfully identified the associated galaxies for 59 out of the 112 sources.

The bottom panel of Fig. 1 shows the distribution of the above-generated sample in galactic coordinates. The sample consists of sources with galactic latitude,  $|b| > 28^\circ$ , which in addition to the GRM removal, has minimal effects of galactic foreground as discussed in Farnes et al. (2014). The 59 sources are associated with background quasars that lie within a redshift range of  $0.452 \leq z_{\text{qso}} \leq 2.275$ . More information regarding these 59 sources is listed in Table 2. It is important to note that our selection process relied on a strict visual inspection, thereby ensuring the absence of any false detection of quasar-galaxy pairs.

<sup>3</sup> <https://skyserver.sdss.org/dr16/en/home.aspx>

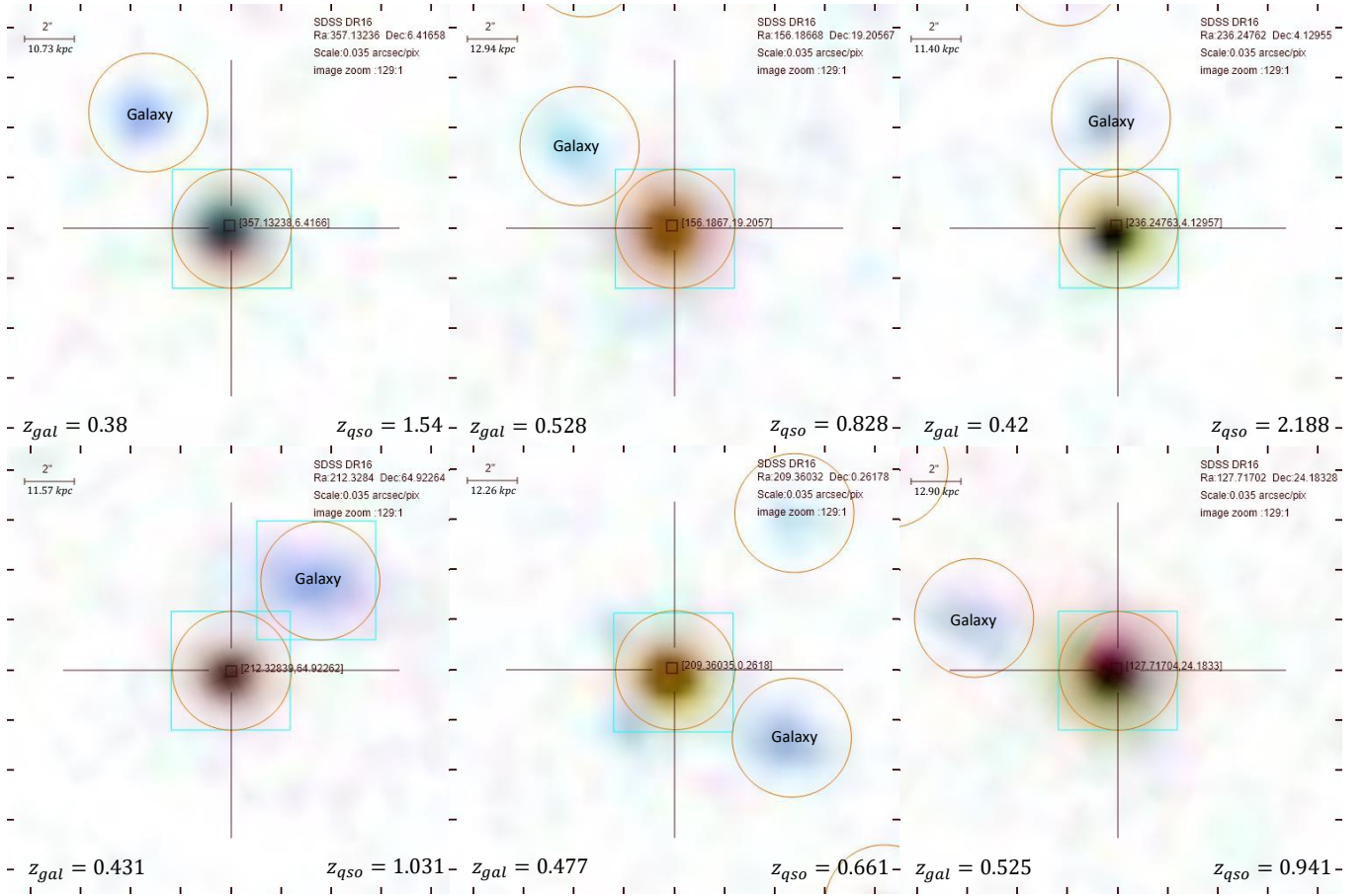


**Figure 2.** The figure shows a sample of 6 sightlines from our sample of 59 sources as extracted from the SDSS Skyserver. These sub-panels of size  $18'' \times 18''$  represent the region of the sky with a quasar in the center. We have taken the closest photometrically identified galaxy in the region (representing our intervening galaxy). We need to note that the sub-sample shown here is quasar-galaxy pairs with low-impact parameters ( $\leq 40$  kpc). Consequently, all the physical quantities, such as impact parameters, are calculated with respect to the intervening galaxy redshift. The quasars are depicted using various colors, which can primarily be attributed to their luminosity, given that they exist at different redshifts. The transverse distance mentioned at the top-left corner of each subpanel is evaluated at the redshift of the galaxy.

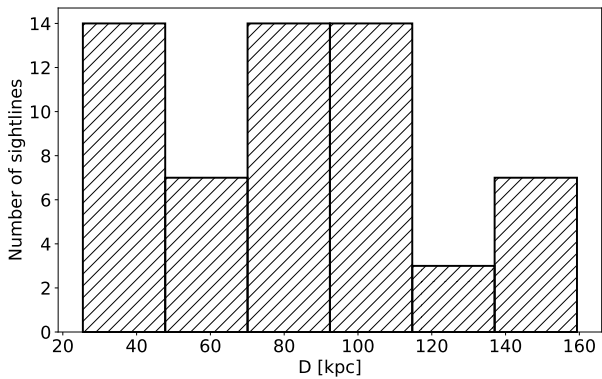


**Figure 3.** The figure shows the histogram of the 59 sources at different impact parameters.

### 3 ANALYSIS AND RESULTS

#### 3.1 ESTIMATION OF IMPACT PARAMETERS

As discussed in Section 1, the magnetic field profiles of many nearby galaxies in the local group of the Milky Way have been much studied

in the literature (for a review see (Beck 2015)). However, the detailed radial profile of the magnetic field for the galaxies at high redshift is not yet well developed. To develop a radial profile of the galactic magnetic field, including the CGM up to 160 kpc, we have utilized our controlled sample of 59 quasar-galaxy pairs. These galaxies have been identified in spectroscopic absorption spectra of the background quasar through the Mg II doublet absorption lines and confirmed by a visual check from the photometric observations. As it is clear from Fig. 2, we can determine the angular separation of the quasar sightline from the center of the galaxy. It is given by

$$\theta = \sqrt{((\Delta\delta)^2 + (\Delta\alpha)^2 \cos^2(\delta_{QSO}))}, \quad (1)$$

where  $\Delta\alpha$  and  $\Delta\delta$  are obtained from the RA & DEC of the quasar LoS and the center of its foreground galaxy. Subsequently, the impact parameter  $D = \theta d_A(z_{gal})$ , wherein  $d_A(z_{gal})$  denotes the angular diameter distance at the redshift of the absorber galaxy (Nielsen et al. 2013). To compute the impact parameter corresponding to the observed angular separation for our quasar-galaxy system at the redshift of the foreground galaxy, we employ the LambdaCDM cosmological

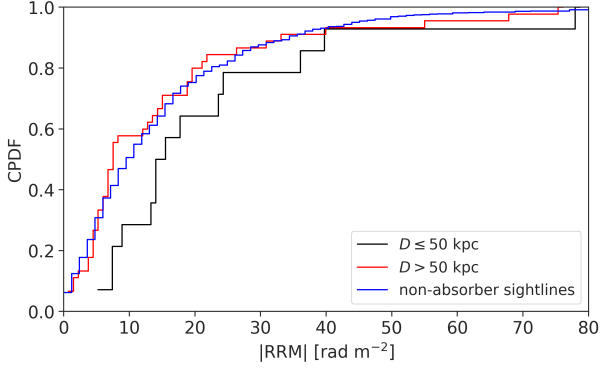


**Figure 4.** Cumulative probability density function of the  $|RRM|$  for two sub-samples binned at 50 kpc. The solid blue line shows the CPDF sightlines with  $D \leq 50$  kpc, whereas the red line shows the CPDF for sightlines having  $D > 50$  kpc. KS test for the three cases: (i)  $D \leq 50$  and  $D > 50$ ; (ii)  $D \leq 50$  and non-absorber sightlines; and (iii)  $D > 50$  and non-absorber sightlines, rejects the null hypothesis at a confidence level of 95%, 90%, and 78%, respectively.

model available in the *Astropy*<sup>4</sup> library, following the framework presented by Hogg (2000). The key cosmological parameters utilized in this model are  $H_0 = 67.74 \text{ km s}^{-1} \text{ Mpc}^{-1}$ ,  $\Omega_m = 0.31$ , and  $\Omega_\Lambda = 0.69$  (Planck Collaboration et al. 2016).

Our sample encompasses a diverse range of impact parameters, from 25 kpc to 160 kpc, with a mean impact parameter of 84 kpc (see Fig. 3). This range of the impact parameter corresponds to the CGM of typical Milky Way-type galaxies.

### 3.2 ESTIMATION OF THE EXCESS RRM AND THE RADIAL PROFILE

As emphasized in Section 1, magnetic fields in any intervening system along the LoS to the source quasar will lead to an RRM excess over and above the IGM and the host contribution. We need to extract this carefully. To account for any redshift evolution in the RRM of quasars, we consider only those non-absorber sightlines with redshifts within the range  $0.452 \leq z_{\text{qso}} \leq 2.275$ . This criterion ensures that the redshift distribution of the selected non-absorber sightlines is consistent with that of the quasars with absorbers in our dataset. Following this redshift matching criterion, we obtain a sub-sample comprising 753 non-absorber sightlines. Utilizing the RRM and the impact parameters of our sample of 59 sightlines, we divide the sample into two sub-samples with impact parameters  $D \leq 50$  kpc and  $D > 50$  kpc. The standard deviations of RRM corresponding to these two sub-samples are  $29.04 \pm 2.62 \text{ rad m}^{-2}$  and  $22.19 \pm 1.33 \text{ rad m}^{-2}$ , respectively. We performed the two-sampled Kolmogorov-Smirnov (KS) test<sup>5</sup> (see Hodges 1958) to check the null hypothesis that these sub-samples are drawn from the same underlying population. A KS test rejects the null hypothesis at a 95% confidence level. We also find that the KS tests for (i)  $D \leq 50$  kpc with non-absorber sightlines, and (ii)  $D > 50$  kpc with non-absorber sightlines rejects the null hypothesis with a confidence level of 90%, and 78%, respectively. Also, it can be seen from the cumulative probability density function in Fig. 4 that the sightlines having  $D \leq 50$  kpc have greater RRM than the sightlines with  $D > 50$  kpc and the non-absorber sightlines.

<sup>4</sup> <https://www.astropy.org/>

<sup>5</sup> <https://real-statistics.com/non-parametric-tests/goodness-of-fit-tests/two-sample-kolmogorov-smirnov-test/>

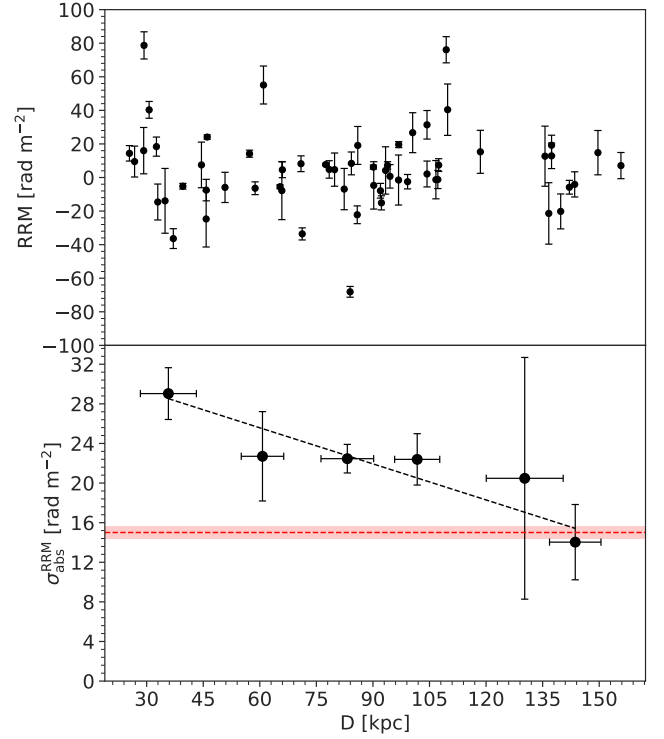


**Figure 5.** *Top Panel:* The figure shows the distribution of the RRM of the sightlines with absorbers with the impact parameter ( $D$ ) for our sample of 59 sightlines. *Bottom Panel:* The  $\sigma_{\text{abs}}^{\text{RRM}}$  shows a decreasing trend with the impact parameter. The linear fitting to  $\sigma_{\text{abs}}^{\text{RRM}}$  vs  $D$  plot (black dashed line) yields a slope of  $-0.12 \pm 0.02 \text{ rad m}^{-2} \text{ kpc}^{-1}$  and an intercept of  $32.87 \pm 1.84 \text{ rad m}^{-2}$ . The horizontal red line with bands represents the  $\sigma_{\text{non-abs}}^{\text{RRM}} = 15.01 \pm 0.6 \text{ rad m}^{-2}$ .

This indicates that the RRM sub-samples have different characteristics with impact parameters and therefore can be used to estimate the radial profile.

In the top panel of Fig. 5, we have plotted the distribution of RRM for sightlines with absorbers, with the impact parameter. The plot suggests that there is a qualitative decrease in RRM with the ‘radial’ distance characterized by the impact parameter (assuming all intervenors are similar and thus this trend will be one for a typical galaxy in the chosen redshift range). To quantify the trend, we proceed by binning the sources in the impact parameter and computing the dispersion of RRM characterized by the standard deviation,  $\sigma_{\text{abs}}^{\text{RRM}}$  in each bin. The uncertainty in  $\sigma_{\text{abs}}^{\text{RRM}}$  for each bin is estimated using the method of propagation of errors as,

$$\delta\sigma_{\text{abs}}^{\text{RRM}} = \frac{\sqrt{\sum_{i=1}^{N_b} [(RRM_i - \langle RRM \rangle)^2 \times ((\delta RRM_i)^2 + (\delta \langle RRM \rangle)^2)]}}{(N_b - 1) \times \sigma_{\text{abs}}^{\text{RRM}}} \quad (2)$$

where  $\langle RRM \rangle$  and  $N_b$  represent the average RRM and number of sources, respectively, in each bin. The trend of  $\sigma_{\text{abs}}^{\text{RRM}}$  with impact parameter is shown in the bottom panel of Fig. 5. We find that the  $\sigma_{\text{abs}}^{\text{RRM}}$  is anti-correlated with the impact parameter having a weighted

Pearson correlation coefficient<sup>6</sup> (Yu & Hutson 2024),  $\rho_p \approx -0.93$ . Even though this anti-correlation is not visually apparent in Fig. 5, however, we explored the linear regression to quantify this anti-correlation. A linear regression including uncertainties yields a slope of  $-0.12 \pm 0.02 \text{ rad m}^{-2} \text{ kpc}^{-1}$  and an intercept of  $32.87 \pm 1.84 \text{ rad m}^{-2}$ . The red dotted line represents the dispersion threshold  $\sigma_{\text{non-abs}}^{\text{RRM}} = 15.01 \pm 0.6 \text{ rad m}^{-2}$  of the 753 non-absorber sightlines. The excess due to intervening absorbers is clearly evident.

For a given single LoS, the  $\delta\text{RRM}$  (error bar) is related to the fluctuations of the small-scale magnetic field. We are interested in the excess due to the large-scale magnetic field. Using the dispersion of the two samples, we estimate the excess RRM due to absorbers  $\sigma_{\text{ex}}^{\text{RRM}}$  (Joshi & Chand 2013) as

$$\sigma_{\text{ex}}^{\text{RRM}} = \sqrt{(\sigma_{\text{abs}}^{\text{RRM}})^2 - (\sigma_{\text{non-abs}}^{\text{RRM}})^2} \quad (3)$$

where the error on  $\sigma_{\text{ex}}^{\text{RRM}}$  given by

$$\delta\sigma_{\text{ex}}^{\text{RRM}} = \frac{1}{\sigma_{\text{ex}}^{\text{RRM}}} \sqrt{(\sigma_{\text{abs}}^{\text{RRM}})^2 (\delta\sigma_{\text{abs}}^{\text{RRM}})^2 + (\sigma_{\text{non-abs}}^{\text{RRM}})^2 (\delta\sigma_{\text{non-abs}}^{\text{RRM}})^2} \quad (4)$$

The upper panel of Fig. 6 shows the variation of the excess RRM with impact parameter. For the last impact parameter bin (140-160 kpc), we place an upper bound on the  $\sigma_{\text{ex}}^{\text{RRM}}$  using the upper limit of the  $1\sigma$  error bar, that is,  $\sigma_{\text{abs}}^{\text{RRM}} + \delta\sigma_{\text{abs}}^{\text{RRM}}$ . We observe that the  $\sigma_{\text{ex}}^{\text{RRM}}$  follows a similar profile as of  $\sigma_{\text{abs}}^{\text{RRM}}$  with the impact parameter having a weighted Pearson correlation coefficient of  $\rho_p \approx -0.94$ . The slope and intercept are found to be  $-0.13 \pm 0.02 \text{ rad m}^{-2} \text{ kpc}^{-1}$  and  $28.53 \pm 1.91 \text{ rad m}^{-2}$  using linear regression. Also, we find  $\sigma_{\text{ex}}^{\text{RRM}}$  for the two sub-samples with  $D \leq 50 \text{ kpc}$  and  $D > 50 \text{ kpc}$  to be  $24.86 \pm 3.08 \text{ rad m}^{-2}$  and  $16.34 \pm 1.88 \text{ rad m}^{-2}$ , respectively. This decreasing radial trend in our analysis is also in line with the investigation by Bernet et al. (2013) and intervening galaxy rotation measure as examined by Lan & Prochaska (2020) for smaller impact parameters.

### 3.3 RADIAL PROFILE OF MAGNETIC FIELD

We obtain the radial profile of the galactic magnetic field using the linear relationship between RRM and the LoS component of the magnetic field strength. The column-averaged strength of the LoS magnetic field is given by (see Eq. 15 in Kronberg et al. 2008)

$$\langle B_{\parallel} \rangle = 0.55 \mu\text{G} \left( \frac{1 + z_{\text{med}}}{3.5} \right)^2 \left( \frac{\sigma_{\text{ex}}^{\text{RRM}}}{20 \text{ rad m}^{-2}} \right) \left( \frac{N_e}{1.7 \times 10^{21} \text{ cm}^{-2}} \right)^{-1} \quad (5)$$

where  $z_{\text{med}}$  is the median redshift of the intervening galaxies lying in a given bin of the impact parameter, and  $N_e$  denotes the electron column density. Using  $\sigma_{\text{ex}}^{\text{RRM}}$ , we obtain the radial profile of the galactic magnetic field as depicted in Fig. 6. Assuming similar properties among all the intervening galaxies within our sample of 59 sightlines, treating them as a single galactic system. For the electron column density, we adopted a value of  $N_e \approx 9 \times 10^{19} \text{ cm}^{-2}$  as reported in Bernet et al. (2008) for a typical galaxy. Our assumption of a nearly constant column density relies on the studies carried out by Afruni (2016) and van de Voort et al. (2018). We note the decreasing trend of  $\langle B_{\parallel} \rangle$  with increasing impact parameter radial distance,

<sup>6</sup> The weighted Pearson correlation coefficient defined by the expression  $\rho_p := \frac{\sum w_i (x_i - \bar{x})(y_i - \bar{y})}{\sqrt{\sum w_i (x_i - \bar{x})^2 \sum w_i (y_i - \bar{y})^2}}$  accounts for the error in the y-datapoints by incorporating weights, where each weight is defined as  $w_i = 1/\delta y_i$ .

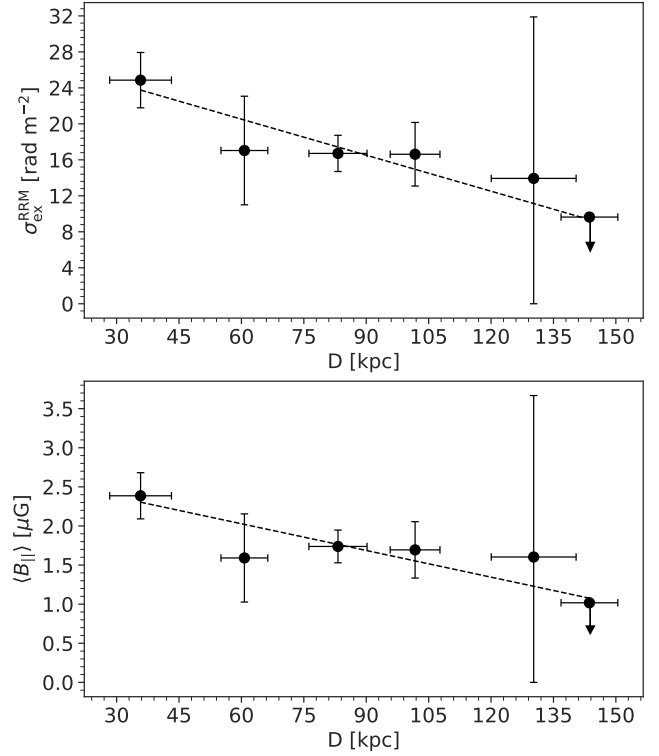


**Figure 6.** *Top Panel:* The figure shows the variation of the  $\sigma_{\text{ex}}^{\text{RRM}}$  with the impact parameter. For the last data point, we have used the upper limit of  $\sigma_{\text{abs}}^{\text{RRM}}$  to fix the upper bound of  $\sigma_{\text{ex}}^{\text{RRM}}$ . The linear fitting yields a slope of  $-0.13 \pm 0.02 \text{ rad m}^{-2} \text{ kpc}^{-1}$  and an intercept of  $28.53 \pm 1.91 \text{ rad m}^{-2}$ . *Bottom Panel:* The plot shows the derived strength of the LoS component of the magnetic field using  $\sigma_{\text{ex}}^{\text{RRM}}$ . The linear fitting yields a slope of  $-0.011 \pm 0.002 \mu\text{G kpc}^{-1}$  and an intercept of  $2.71 \pm 0.194 \mu\text{G}$ . Note that the expression for  $\langle B_{\parallel} \rangle$  as given in Eq. 5 will always give a positive magnetic field, which is why we have constrained the given plot to be above the x-axis.

similar to  $\sigma_{\text{ex}}^{\text{RRM}}$  as we traverse into the circumgalactic medium of a typical milky-way type galaxy at a median redshift  $z = 0.55$ .  $\langle B_{\parallel} \rangle$  and the impact parameter  $D$  are anti-correlated with a weighted Pearson correlation coefficient of  $\rho_p \approx -0.89$ . The linear fitting yields a slope of  $-0.011 \pm 0.002 \mu\text{G kpc}^{-1}$  and an intercept of  $2.711 \pm 0.194 \mu\text{G}$ .

We have observed that the CGM exhibits a magnetic field with strengths exceeding  $2\mu\text{G}$  near the galactic disc ( $\sim 35 \text{ kpc}$ ), gradually decreasing radially. This observation aligns well with the findings of Pakmor et al. (2020), where the authors conducted a similar examination in simulation studies. Furthermore, a recent study by Jung et al. (2023), employing the large cosmological simulation IllustrisTNG50 and a comprehensive galaxy catalog, has probed the magnetic field in high-velocity clouds within the CGM. This study reports substantial magnetic field strengths in these clouds with a radial decrease (see Fig. A1 in Jung et al. 2023). Our observational analysis, based on the rotation measure of background quasars, directly confirms such radial magnetic field profile within the CGM of the galaxies.

It is crucial to emphasize that our primary focus lies in comparing our observations with the aforementioned simulations. Since the simulations are conducted in a 3D magnetic field model, a direct comparison alone may not suffice for drawing meaningful conclusions. Our analysis yields average LoS magnetic field strengths of  $2.53 \pm 0.31 \mu\text{G}$  and  $1.66 \pm 0.19 \mu\text{G}$  for sightlines having impact

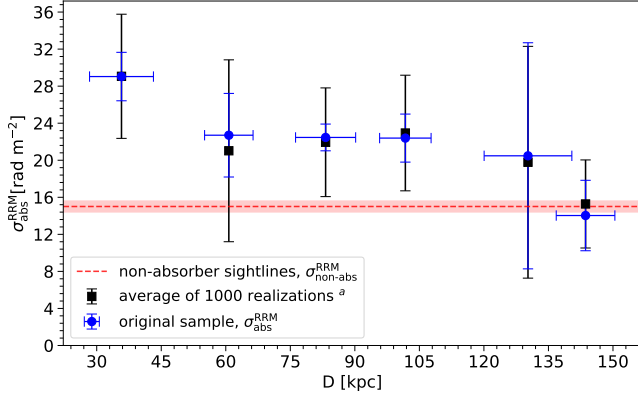


**Figure 7.** The figure shows the variation of  $\sigma_{\text{abs}}^{\text{RRM}}$  with the impact parameter D for two different cases (i) simulated datasets (black), and (ii) real observations (blue). <sup>a</sup> We have estimated  $\sigma_{\text{abs}}^{\text{RRM}}$  for 1000 simulated realizations and calculated the average over all the realizations. The details of the simulated dataset are given in Section 3.4.

parameters  $D \leq 50$  kpc and  $D > 50$  kpc, respectively. This suggests a clear indication of varying magnetic field from disk to the CGM. The average magnetic field estimated from the excess RRM for the 59 sightlines is  $\langle B_{\parallel} \rangle \sim 1.88 \pm 0.16 \mu\text{G}$  at a median redshift of  $z_{\text{med}} = 0.55$ . Additionally, our estimated average magnetic field for the CGM is consistent with the constraints imposed by Lan & Prochaska (2020).

We note that the obtained impact parameters primarily sample the halo and CGM of the galaxy. Visual inspections and the SDSS classification revealed no complexity in the foreground galaxies, such as merging systems. Therefore, we have assumed that inclination and morphological effects are minimal in this first stride. We plan to include these effects in future investigations.

### 3.4 VALIDATION USING SIMULATED REALIZATIONS

To strengthen the confidence level of the rotation measure radial profile, we have checked into the simulated RRM observations. The procedure for generating synthetic observations is given below;

(i) In real observations, we have 59 sightlines with given RRM and their respective error  $\delta\text{RRM}$ . We generated a sample of 1000 data points corresponding to each sightline assuming a Gaussian distribution with mean and standard deviation given by the RRM and  $\delta\text{RRM}$  of sightline, respectively.

(ii) As each of the 59 sightlines is associated with an impact parameter, we hence have 1000 realizations corresponding to each impact parameter from the above step. We randomly selected one simulated RRM from the respective set of 1000 values, for every original sightline, bin by bin in the impact parameter. For example, in the first impact parameter bin, we had originally 14 sources, which in turn, gave us 1000 simulated RRM values each. We selected an RRM value at random from each of these 1000 values to obtain 14 simulated values for the first bin. This procedure is repeated for all the bins.

(iii) We computed the dispersion in the simulated RRM values, denoted by  $\sigma_{\text{abs(sim)}}^{\text{RRM}}$ . We repeated step (ii) to have 1000 realizations of  $\sigma_{\text{abs(sim)}}^{\text{RRM}}$ , and finally computed the average of these 1000 values.

In Fig. 7, we have plotted the averaged  $\sigma_{\text{abs(sim)}}^{\text{RRM}}$  for each bin

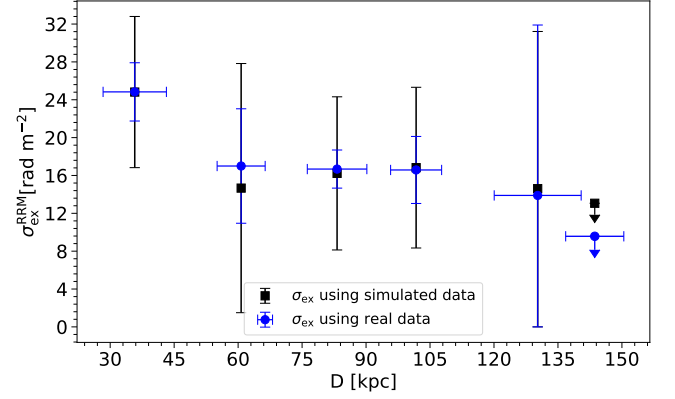


**Figure 8.** The figure shows the variation of  $\sigma_{\text{ex}}^{\text{RRM}}$  estimated using (i) simulated data,  $\sigma_{\text{abs(sim)}}^{\text{RRM}}$  (black), and (ii) real observations,  $\sigma_{\text{abs}}^{\text{RRM}}$  (blue), with the impact parameter D. The last data point for both cases is estimated as an upper bound on the  $\sigma_{\text{ex}}^{\text{RRM}}$  using the upper limit of the  $1\sigma$  error bar, that is,  $\sigma_{\text{abs}}^{\text{RRM}} + \delta\sigma_{\text{abs}}^{\text{RRM}}$  and  $\sigma_{\text{abs(sim)}}^{\text{RRM}} + \delta\sigma_{\text{abs(sim)}}^{\text{RRM}}$  for real observations and simulated data, respectively.

(black) with the impact parameter, in comparison with our real data,  $\sigma_{\text{abs}}^{\text{RRM}}$  (blue). The red line with band represents the  $\sigma_{\text{non-abs}}^{\text{RRM}}$  with its uncertainty  $\delta\sigma_{\text{non-abs}}^{\text{RRM}}$ . We find that the simulated radial profile corroborates the results of Section 3.2, strongly indicating that the effect is real. The error bars on the simulated data points ( $\delta\sigma_{\text{abs(sim)}}^{\text{RRM}}$ ) represent the  $1\sigma$  (standard deviation) range of the simulated RRM dispersion. This indicates that the real data points lie within 68% of the simulated data. In addition, we compute and plot the excess RRM in our simulated dataset (black) in Fig. 8 along with the excess coming from real data (blue); both exhibit a similar decreasing radial profile confirming our technique and study with the real dataset.

## 4 DISCUSSION

Magnetic fields in the high redshift galactic systems have been probed using the polarized background quasar sightlines and their rotation measures. As mentioned before, RM is an integrated effect with contributions from the host environments, any intervening systems, the IGM, and our own galaxy, the Milky Way. We have inferred the radial profile of the magnetic field in a typical high redshift galaxy and its CGM in one of the first-of-a-kind investigations using an ensemble of quasar-galaxy pairs. Our methodology is an advancement over some of the previous strides in this direction. Our results are in agreement with the investigations in the nearby galaxies and also put forward observational evidence to results in a recent study (Jung et al. 2023) coming from the cosmological simulation studies. Before presenting the final conclusion of our study, we shall now briefly discuss these aspects.

In many previous investigations, the excess in RM (or RRM) due to the Mg II absorbers has been used to estimate the strength of the LoS component of magnetic fields in high redshift galaxies. For instance, Bernet et al. (2008) utilized their 71 sources with RM measurements at 6 cm and reported magnetic fields of the order of about  $10\mu\text{G}$ . Additionally, Kronberg et al. (2008) performed an analysis with 268 sources by considering the exclusion of the galactic contribution to RM. The authors estimated an order of magnitude to be approximately  $1\mu\text{G}$ . This discrepancy in the order estimate could be due to the different sizes of the dataset and the directional de-

pendence of GRM which has not been considered by [Bernet et al. \(2008\)](#). [Bernet et al. \(2010\)](#) using the RM data at 21 cm from the catalog compiled by [Taylor et al. \(2009\)](#) also did not find any correlation of Mg II absorbers with RM. This concern was mitigated in the subsequent studies; for example, [Farnes et al. \(2014\)](#) examined 599 sources based on the radio morphology of the background quasars with RM values at 21 cm. The authors found that the intervening Mg II systems show an excess RM in flat spectrum sources and host magnetic fields of average strength of approximately  $1.8 \pm 0.4 \mu\text{G}$ . Later [Malik et al. \(2020\)](#) compiled a comparatively larger catalog of 1132 sources using 21 cm RM data and obtained a significant excess in RRM associated with the Mg II absorbers. The authors also carried out an analysis based on the spectral index and found an excess RRM in flat-spectrum sources, agreeing with [Farnes et al. \(2014\)](#). This removed the above discrepancy among the 6 cm and 21 cm RM data. However, [Bernet et al. \(2012\)](#) discussed the above discrepancy using their model of depolarisation due to inhomogeneous Faraday screens. The authors carried out their analysis with 54 sources from [Bernet et al. \(2008\)](#) and studied the wavelength-dependent depolarisation effects with 6cm and 21cm polarization data. The analysis showed that the presence of intervening absorbers is associated with depolarization. Also, [Kim et al. \(2016\)](#) thoroughly examined a sample of 49 sources from [Bernet et al. \(2008\)](#) by the technique of RM synthesis. Their results also established a connection between the intervening absorbers and depolarization. [Malik et al. \(2020\)](#) found no significant difference between the fractional polarisation of the sources with and without absorbers suggesting that the major contribution to depolarization is due to the environment of the host (also taken up in a recent article by [Taylor et al. \(2023\)](#)). By utilizing the 1132 sources, [Malik et al. \(2020\)](#) found the average field strength by using excess RRM to be approximately  $1.3 \pm 0.3 \mu\text{G}$ . Our finding supports these previous investigations. We determined that the average strength of the LoS magnetic field of  $1.88 \pm 0.16 \mu\text{G}$ . Our work goes ahead by also considering the contribution to RRM from the host environment, and advancing a methodology to remove the same to obtain purely the contribution from the intervening galaxy in terms of  $\sigma_{\text{ex}}^{\text{RRM}}$ . Also, we undertook special care in the identification of the galaxies. All the sources have been analyzed carefully with a visual check, and no automated search has been involved.

The structure of the galactic magnetic fields has been well probed in the case of the Milky Way and the nearby galaxies. On a scale of qualitative analysis, our findings agree well with the previous investigations on milky-way galaxy ([Seta & Federrath 2021](#)), and nearby galaxies ([Beck 2015](#)). We even find a similar trend as obtained in the cosmological simulations performed by (see refs. [Pakmor et al. 2017, 2020; Jung et al. 2023](#)). In some earlier attempts to probe the radial profile of the magnetic fields in the high- $z$  galaxies, for instance, [Bernet et al. \(2013\)](#) inferred a similar rundown of magnetic fields with an impact parameter distribution up to about 50 kpc for 28 sightlines using RM observations at 6 cm. We have avoided mixing our sample (RM observations at 21 cm) with their sources at the 6 cm wavelength to maintain the homogeneity in the frequency of our sample. Further, their analysis emphasizes that the RM beyond 50 kpc is negligible. However, the coverage of impact parameters in our sample is comparatively much larger and well supported by the fact that CGM has a very high covering fraction up to 200 kpc (see refs. [Bordoloi et al. 2018; Lan & Prochaska 2020](#)). Recently, [Böckmann, K. et al. \(2023\)](#) have studied the RM of 125 high redshift galaxies from the COSMOS and XMM-LSS fields with a median redshift of the collective sample of 0.42. The authors analyzed their sources up to 400 kpc and found that the galaxies in the COSMOS field with  $D < 133$  kpc show an excess in the median  $|\text{RM}|$  of  $2.5 \pm 1.1 \text{ rad m}^{-2}$

as compared to the galaxies with  $D > 133$  kpc, and for XMM-LSS, the galaxies with  $D < 266$  kpc show an excess of  $5.0 \pm 2.3 \text{ rad m}^{-2}$ . Thus, both the samples collectively result in a redshift corrected excess of  $5.6 \pm 2.3 \text{ rad m}^{-2}$ , using which they obtained a magnetic field strength of  $0.48 \mu\text{G}$ . Also, [Heesen, V. et al. \(2023\)](#) have probed magnetic fields in the CGM of nearby galaxies up to 1000 kpc based on a classification of sources on the basis of the inclination of the quasars' position with respect to the minor axis of the galaxies. Only those galaxies having quasars near the minor axis ( $< 45^\circ$ ) show a steep decrease in the  $|\text{RRM}|$  up to 100 kpc. A similar analysis was carried out by [Bordoloi et al. \(2011\)](#), exploring the azimuthal profiles of Mg II absorption. This indicates the presence of magnetized bipolar winds in the galaxies in the nearby galaxies. Due to the low spatial resolution in SDSS at high redshifts, it is difficult to obtain any information about the morphology and orientation of our absorber galaxies. High-resolution observations are required to carry out an investigation on the bipolar winds in high redshift galaxies, which we will be using in follow-up work.

We do note that finer details in our analysis are also limited by the current dataset of RM observations. However, it is anticipated that future polarimetric surveys, such as the Square Kilometre Array ([Heald et al. 2020](#)), will help by supplying much more accurate RM data with a significantly higher number density of radio sources. In addition, the new measurements from spectroscopic and photometric surveys such as the SDSS and Dark Energy Spectroscopic Instrument (DESI<sup>7</sup>) ([Dey et al. 2019](#)) are anticipated to open up a new avenue towards comprehending the galactic magnetic fields.

## 5 CONCLUSION

In summary, our study focused on developing a probe to investigate the morphology of magnetic fields in high-redshift galaxies. We achieved this by utilizing the rotation measure of quasars whose sightlines intersect with the magnetized plasma of foreground galaxies. The key findings are as follows:

(i) We have developed a sample of optically confirmed 59 quasars having a single Mg II absorber associated with intervening foreground galaxies within a redshift range of  $0.372 \leq z_{\text{abs}} \leq 0.8$ . We have verified these galaxies using photometric as well as spectroscopic redshift with the  $3\sigma_{z\text{-photo}}$  limit.

(ii) To calculate the RM contribution of the intervening galaxies, we began with RRM ( $\text{RRM} = \text{RM} - \text{GRM}$ ), which has the Milky Way contributions already removed for all the sightlines, with and without the absorbers. We then found the excess in the dispersion of RRM, i.e.,  $\sigma_{\text{ex}}^{\text{RRM}}$  by subtracting the absorber and non-absorber dispersion in quadrature.

(iii) After dividing the sample of 59 sightlines into two sub-samples with  $D \leq 50$  kpc and  $D > 50$  kpc, we found, the excess RRM quantified by  $\sigma_{\text{ex}}^{\text{RRM}}$  to be  $24.86 \pm 3.08 \text{ rad m}^{-2}$  and  $16.34 \pm 1.88 \text{ rad m}^{-2}$ , respectively.

(iv) We translated the excess RRM into magnetic field  $\langle B_{\parallel} \rangle$  considering a typical electron column density,  $N_e \approx 9 \times 10^{19} \text{ cm}^{-2}$ . In these two sub-samples with  $D \leq 50$  kpc and  $D > 50$  kpc,  $\langle B_{\parallel} \rangle$  is found to be  $2.53 \pm 0.31 \mu\text{G}$  and  $1.66 \pm 0.19 \mu\text{G}$ . This suggests a clear indication of the radially decreasing magnetic field in a typical galaxy from disk to CGM.

Our study provides a comprehensive investigation of the magnetic

<sup>7</sup> <https://www.desi.lbl.gov/>



field in the high-redshift galaxies. It can serve as a valuable precursor for ongoing and forthcoming RM surveys, including VLASS, LOFAR, and SKA.

## ACKNOWLEDGMENTS

The research of S.S. is supported by the Young Faculty Incentive from the Indian Institute of Technology Delhi, India, and the Core Research Grant CRG/2021/003053 from the Science and Engineering Research Board, India. Research of S.B. is supported by the Insitute Fellowship from the Indian Institute of Technology Delhi, India. We are grateful to the anonymous referee for providing insightful comments that significantly contributed to the enhancement of our manuscript.

Funding for the Sloan Digital Sky Survey V has been provided by the Alfred P. Sloan Foundation, the Heising-Simons Foundation, the National Science Foundation, and the Participating Institutions. SDSS acknowledges support and resources from the Center for High-Performance Computing at the University of Utah. The SDSS web site is [www.sdss.org](http://www.sdss.org). SDSS is managed by the Astrophysical Research Consortium for the Participating Institutions of the SDSS Collaboration, including the Carnegie Institution for Science, Chilean National Time Allocation Committee (CNTAC) ratified researchers, the Gotham Participation Group, Harvard University, Heidelberg University, The Johns Hopkins University, L'Ecole polytechnique fédérale de Lausanne (EPFL), Leibniz-Institut für Astrophysik Potsdam (AIP), Max-Planck-Institut für Astronomie (MPIA Heidelberg), Max-Planck-Institut für Extraterrestrische Physik (MPE), Nanjing University, National Astronomical Observatories of China (NAOC), New Mexico State University, The Ohio State University, Pennsylvania State University, Smithsonian Astrophysical Observatory, Space Telescope Science Institute (STScI), the Stellar Astrophysics Participation Group, Universidad Nacional Autónoma de México, University of Arizona, University of Colorado Boulder, University of Illinois at Urbana-Champaign, University of Toronto, University of Utah, University of Virginia, and Yale University.

This work made use of Astropy:<sup>8</sup> a community-developed core Python package and an ecosystem of tools and resources for astronomy (Astropy Collaboration et al. 2013, 2018, 2022).

## DATA AVAILABILITY

We have used the publicly available catalog of 1132 quasars from Malik et al. (2020) and sky images from the SDSS Skyserver. The final dataset of 59 quasar sightlines having foreground galaxies is provided as the supplementary file containing the observed and derived parameters.

## REFERENCES

- Abazajian K. N., et al., 2009, *ApJS*, 182, 543  
 Abolfathi B., et al., 2018, *ApJS*, 235, 42  
 Afruni A., 2016, PhD thesis, <http://amslaurea.unibo.it/12824/>  
 Ahn C. P., et al., 2012, *ApJS*, 203, 21  
 Alam S., et al., 2015, *ApJS*, 219, 12  
 Astropy Collaboration et al., 2013, *A&A*, 558, A33  
 Astropy Collaboration et al., 2018, *AJ*, 156, 123  
 Astropy Collaboration et al., 2022, *apj*, 935, 167  
 Beck R., 2005, *Magnetic Fields in Galaxies*. Springer Berlin Heidelberg, Berlin, Heidelberg, doi:10.1007/3540313966\_3  
 Beck R., 2015, *A&ARv*, 24  
 Beck R., Wielebinski R., 2013, in Oswald T. D., Gilmore G., eds., Vol. 5, *Planets, Stars and Stellar Systems. Volume 5: Galactic Structure and Stellar Populations*. p. 641, doi:10.1007/978-94-007-5612-0\_13  
 Beck, Rainer 2015, *A&A*, 578, A93  
 Bergeron J., Boissé P., 1991, *A&A*, 243, 344  
 Bernet M. L., Miniati F., Lilly S. J., Kronberg P. P., Dessauges-Zavadsky M., 2008, *Nature*, 454, 302 – 304  
 Bernet M. L., Miniati F., Lilly S. J., 2010, *ApJ*, 711, 380  
 Bernet M. L., Miniati F., Lilly S. J., 2012, *ApJ*, 761, 144  
 Bernet M. L., Miniati F., Lilly S. J., 2013, *ApJL*, 772, L28  
 Bordoloi R., et al., 2011, *ApJ*, 743, 10  
 Bordoloi R., Prochaska J. X., Tumlinson J., Werk J. K., Tripp T. M., Burchett J. N., 2018, *ApJ*, 864, 132  
 Brandenburg A., Subramanian K., 2005, *Physics Reports*, 417, 1  
 Böckmann, K. et al., 2023, *A&A*, 678, A56  
 Chen H.-W., Wild V., Tinker J. L., Gauthier J.-R., Helsby J. E., Shectman S. A., Thompson I. B., 2010, *ApJ*, 724, L176  
 Churchill C. W., Mellon R. R., Charlton J. C., Jannuzi B. T., Kirhakos S., Steidel C. C., Schneider D. P., 2000, *ApJS*, 130, 91  
 Crutcher R. M., 2012, *ARA&A*, 50, 29  
 Dey A., et al., 2019, *AJ*, 157, 168  
 Dickey J. M., et al., 2022, *ApJ*, 940, 75  
 Farnes J. S., O'Sullivan S. P., Corrigan M. E., Gaensler B. M., 2014, *ApJ*, 795, 63  
 Gießbübel, R. Heald, G. Beck, R. Arshakian, T. G. 2013, *A&A*, 559, A27  
 Hammond A. M., Robshaw T., Gaensler B. M., 2013 ([arXiv:1209.1438](https://arxiv.org/abs/1209.1438))  
 Han J., 2012, *Proceedings of the IAU*, 8, 223–228  
 Heald G., et al., 2020, *Galaxies*, 8  
 Heesen, V. et al., 2023, *A&A*, 670, L23  
 Henriksen R. N., Irwin J. A., 2016, *MNRAS*, 458, 4210  
 Hodges J. L., 1958, *Arkiv for Matematik*, 3, 469  
 Hogg D. W., 2000 ([arXiv:astro-ph/9905116](https://arxiv.org/abs/astro-ph/9905116))  
 Jansson R., Farrar G. R., 2012, *ApJ*, 757, 14  
 Joshi R., Chand H., 2013, *MNRAS*, 434, 3566  
 Jung S. L., McClure-Griffiths N. M., Pakmor R., Ma Y. K., Hill A. S., Eck C. L. V., Anderson C. S., 2023, Sampling Faraday rotation sky of IllustrisTNG50: I. Imprint of the magnetised circumgalactic medium around Milky Way-like galaxies ([arXiv:2307.05808](https://arxiv.org/abs/2307.05808))  
 Kacprzak G. G., Churchill C. W., Steidel C. C., Murphy M. T., 2008, *AJ*, 135, 922  
 Khoperskov, Sergey A. Khrapov, Sergey S. 2018, *A&A*, 609, A104  
 Kim K. S., Lilly S. J., Miniati F., Bernet M. L., Beck R., O'Sullivan S. P., Gaensler B. M., 2016, *ApJ*, 829, 133  
 Kimball A. E., Željko Ivezić 2008, *AJ*, 136, 684  
 Klein U., Fletcher A., 2015, *Galactic and Intergalactic Magnetic Fields*, doi:10.1007/978-3-319-08942-3.  
 Kronberg P. P., Perry J. J., 1982, *ApJ*, 263, 518  
 Kronberg P. P., Bernet M. L., Miniati F., Lilly S. J., Short M. B., Higdon D. M., 2008, *ApJ*, 676, 70  
 Krumholz M. R., Telles E., Dupke R., Lazzaro D., 2011, in AIP Conference Proceedings. AIP, pp 9–57, doi:10.1063/1.3636038  
 Kulsrud R. M., Cen R., Ostriker J. P., Ryu D., 1997, *ApJ*, 480, 481  
 Lan T.-W., Prochaska J. X., 2020, *MNRAS*, 496, 3142  
 Malik S., Chand H., Seshadri T. R., 2020, *ApJ*, 890, 132  
 Mora-Partiarroyo S. C., et al., 2019, *A&A*, 632, A11  
 Mshar A. C., Charlton J. C., Lynch R. S., Churchill C., Kim T.-S., 2007, *ApJ*, 669, 135  
 Narayanan A., Charlton J. C., Misawa T., Green R. E., Kim T.-S., 2008, *ApJ*, 689, 782  
 Nestor D. B., Turnshek D. A., Rao S. M., 2005, *ApJ*, 628, 637  
 Nielsen N. M., Churchill C. W., Kacprzak G. G., Murphy M. T., 2013, *ApJ*, 776, 114  
 Pakmor R., et al., 2017, *MNRAS*, 469, 3185  
 Pakmor R., et al., 2020, *MNRAS*, 498, 3125  
 Planck Collaboration et al., 2016, *A&A*, 594, A13

<sup>8</sup> <http://www.astropy.org>

- Rees M. J., 1987, *QJRAS*, 28, 197
- Rieder M., Teyssier R., 2016, *MNRAS*, 457, 1722
- Ruzmaikin A. A., Shukurov A. M., Sokoloff D. D., 1988, *Origin of Magnetic Fields*. Springer Netherlands, doi:10.1007/978-94-009-2835-0\_5
- Seta A., Federrath C., 2020, *MNRAS*, 499, 2076
- Seta A., Federrath C., 2021, *MNRAS*, 502, 2220–2237
- Shu F. H., 1992, *Physics of Astrophysics*, Vol. II. University Science Books, <https://ui.adsabs.harvard.edu/abs/1992phas.book.....S>
- Singh V., Chand H., 2018, *MNRAS*, 480, 1796
- Subramanian K., 2008, *Magnetizing the universe* (arXiv:0802.2804)
- Surgent W. J., Lopez-Rodriguez E., Clark S. E., 2023 (arXiv:2302.07278)
- Taylor A. R., Stil J. M., Sunstrum C., 2009, *ApJ*, 702, 1230
- Taylor A. R., et al., 2023, *MIGHTEE Polarization Early Science Fields: The Deep Polarized Sky* (arXiv:2312.13230)
- Thomas T., Pfrommer C., Pakmor R., 2022, *Cosmic ray-driven galactic winds: transport modes of cosmic rays and Alfvén-wave dark regions* (arXiv:2203.12029)
- Tinker J. L., Chen H.-W., 2010, *ApJ*, 709, 1
- Tumlinson J., Peebles M. S., Werk J. K., 2017, *ARA&A*, 55, 389
- Widrow L., 2002, *Reviews of Modern Physics*, 74
- Yu H., Hutson A. D., 2024, *Journal of Applied Statistics*, 51, 481
- van de Voort F., Bieri R., Pakmor R., Gómez F. A., Grand R. J. J., Marinacci F., 2021, *MNRAS*, 501, 4888
- van de Voort F., Springel V., Mandelker N., van den Bosch F. C., Pakmor R., 2018, *MNRAS: Letters*, 482, L85–L89

This paper has been typeset from a  $\text{\TeX}/\text{\LaTeX}$  file prepared by the author.